INT 204/02 February 2002

TOMOGRAPHIC RECONSTRUCTION OF RADIATION INTENSITY PROFILES FROM BOLOMETRIC MEASUREMENTS ON THE TCV TOKAMAK

S. Kalvin, S. Zoletnik

Tomographic reconstruction of radiation intensity profiles from bolometric measurements on the TCV tokamak

S. Kálvin, S. Zoletnik
CAT-SCIENCE Bt.
Detrekő u 1/b H-1022 Budapest, Hungary
manager@catscience.kfkipark.hu
www.catscience.kfkipark.hu

Contents

1 Introduction 2

2 The base function system 2

3 Calculation of the measurement matrix 7

4 Reconstruction method 10

5 Reconstruction tests 11
5.1 Radiation profiles composed of base functions 11
5.2 Other radiation profiles 14

6 The effect of neutral particles 15

7 Reconstruction of plasma discharges 17

8 Using the Graphical User Interface 19

9 Program routines 21

1 Introduction

This report describes a method and software for the reconstruction of the twodimensional radiation intensity distributions in a toroidal cross-section of the TCV tokamak from bolometric data. These measurements are done with a 64 channel 5-camera bolometer camera system. This work constitutes step 2 of contract TCV-TCVXTI-C between CRPP-EPFL, Lausanne and CAT-SCIENCE Bt, Budapest, Hungary. Step 1 of this contract aimed at the reconstruction of the soft X-ray radiation profile within the Last Closed Flux Surface (LCFS) of the plasma using measurements of a soft X-ray camera system.

Both reconstruction techniques make heavy use of the plasma flux surface contour shapes determined from magnetic measurements and equilibrium calculations. The difference between the X-ray tomography and the bolometer tomography method lies in the fact that X-ray radiation profiles are expected to be slowly changing along the magnetic surfaces and negligible outside the LCFS, while in the case of the bolometry measurements strong local radiation sources are expected at the edge of the plasma and in the Scrape Off Layer (SOL). For a description of the X-ray tomography method please see document "Extension of the TCVXTI software package".

Despite the above difference both X-ray and bolometer tomography is based on three common ideas:

- The radiation intensity distribution is built up as a weighted sum of twodimensional functions of a *base function system.*
- First order linear regularisation (see e.g. [1]) is used for selecting reasonable solutions.
- An error bar is attached to all measurement data and the radiation profile is fitted in a way to keep $\chi = 1$.

The difference between bolometer and X-ray tomography is in the base function system and to some extent in the regularisation. Inside the LCFS both methods use the same base function systems, the difference is in the SOL and at the plasma wall, this way bolometer tomography can be considered as an extension of X-ray tomography outside the LCFS.

2 The base function system

The full base function system of the bolometer tomography is composed of three sets of base functions:

1. the base function system of the X-ray tomography (grid type only) is used inside the LCFS (central base function set),
2. around the LCFS and along the "legs" of the separatrix pixels are used whose shape is fitted to the shape of the flux contours (separatrix base function set),
3. a set of pixels is placed along the walls (wall base function set).

All three base function sets are designed in a way that individual base functions have a pyramid-like shape, that is they are 1 at one point (base point) and are linearly interpolated to zero on a polygon surrounding the base point (edge polygon). The sides of the polygon might be curved. Neighbouring base functions are overlapping, thus adding them produces linear

interpolation between the base points. The idea is shown in one dimension on *Fig 1.* Adding the base functions with equal weight a constant function results, while a weighted sum produces a function composed of broken lines. The value at the base points of the base functions equals the weight of the corresponding base function.

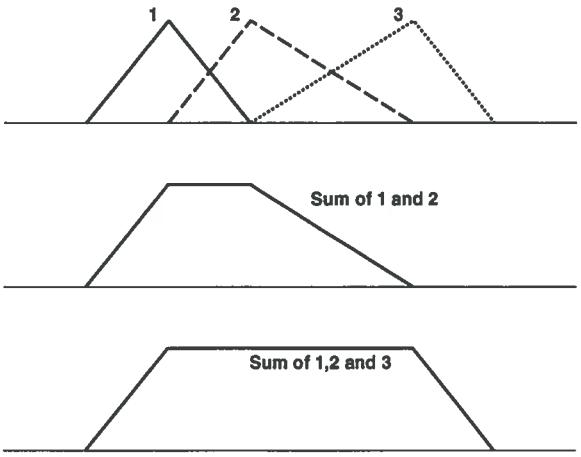

Fig. 1. Explanation for the addition of base functions.

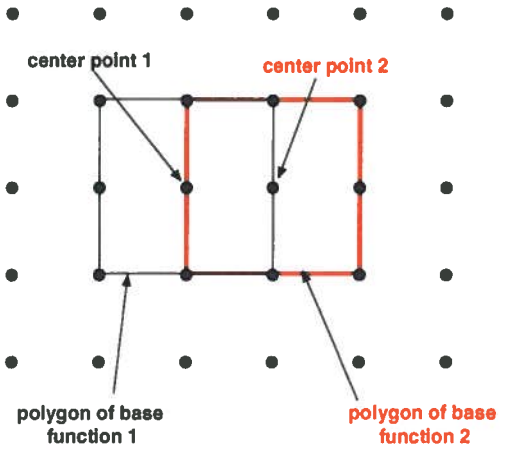

Fig. 2. Arrangement of two neighbouring base functions in case of a regular twodimensional set of base points.

The three base function sets differ in the way how their edge polygon looks. For the central base function set the polygons are distorted rectangles as show on *Fig. 2.* In the base point the base function is one and it is bilinearly interpolated to 0 at the edge polygon. Such base functions are applicable where the plane is covered by a regular grid of points which can be arranged into rows and columns. The lines connecting the rows and columns needn't be straight but can be curved to an arbitrary shape. Inside the separatrix the row of points follow the flux contours, thus these base functions can easily represent radiation profiles which follow the shape of the flux contours.

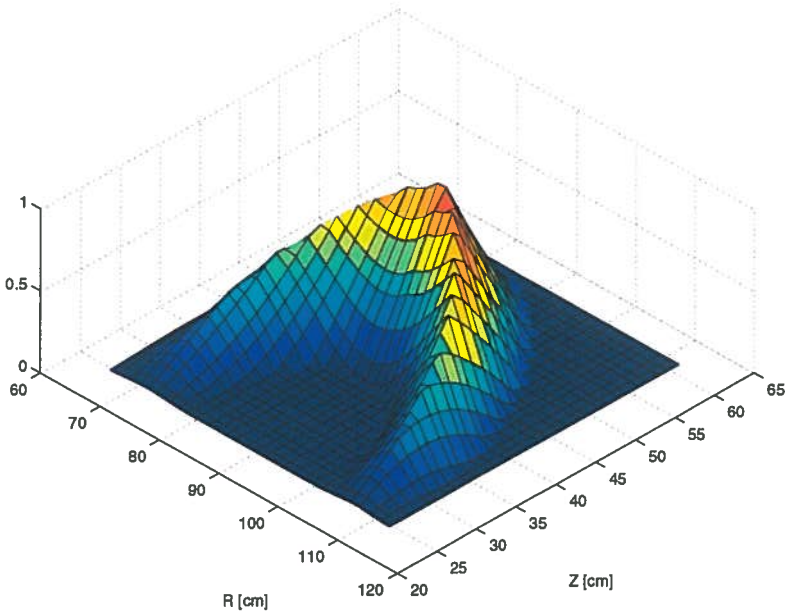

Fig. 3. Surface plot of a central base function.

There is one extraordinary point in this scheme, namely the magnetic axis. This could be treated separately, but in a way that the linear interpolation between the base points is kept. For more details of this base function set please refer to the X-ray tomographic reconstructions. A central base function is shown on *Fig. 3.* Its edge polygon is a rectangle bent onto the shape of a flux contour.

The central base function set is generated by selecting a certain number (`n_rad`) of radial zones by taking equidistant flux values between the separatrix and the magnetic axis. In each zone a certain number (`n_pol`) of base points are arranged poloidally equidistantly. The innermost zone is not divided poloidally it contains a single hat-like base function, whose base point is the magnetic axis.

This base function set does not work if the base points cannot be arranged into rows and columns. This is the case at the X-points of the magnetic configuration. The problem arises from the fact that an arbitrary set of 2D points cannot be arranged to quadrangles. On the other hand an arbitrary set of points can be triangulated, that is the plane is covered by triangles whose corners are the points. Base functions can be built by selecting a base point and building the edge polygon by unifying all triangles surrounding the base point. Examples are shown on *Fig. 4.* The two cases show different triangulations for the same point set. As it can be seen the base functions defined this way are not defined alone by the point set but their shape also depend on the triangulation method. The edge polygons of the base functions are quadrangles, pentagons, ... and interpolation is done within their sub-triangles. The value of the base function changes linearly between the three corner points of each triangle. Once the triangulation of the points is fixed the weighted sum of the base functions will create a function whose value changes linearly within each triangle. At the corner points the value will be equal to the weight of the base function of which the corner point is its base point.

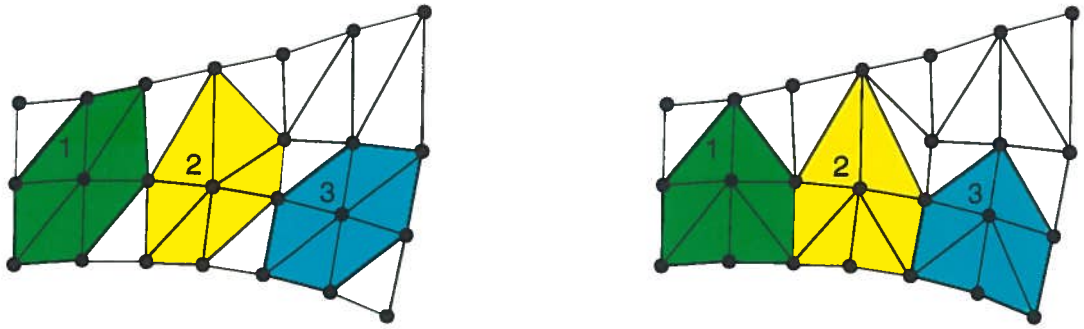

Fig. 4. Some base functions for the same point set and base points but different triangulation.

If the base points are arranged systematically it is worth doing the triangulation also in a systematic way and thus controlling the shape of the base functions. In the edge region of the TCV magnetic configurations the base points can be arranged in rows along the magnetic flux contours and in columns perpendicular to them. This forms a regular structure except at the x-points. An example base function for such a regular point set is shown on *Fig. 5(a).* The base function is not aligned along the flux contours but has an inclination. To avoid this strange behaviour the consecutive rows of points are shifted by half point distance and this way the base functions can be transformed to hexagons as it is shown on *Fig. 5(b).* The overlapping hexagonal base functions form most of the separatrix base function set. At the x-points these are connected to other polygons. Examples are shown on *Figs. 6,7.*

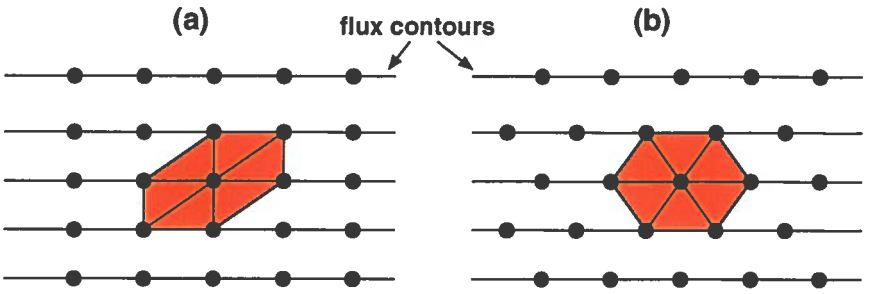

Fig. 5. Base functions for two different point set arrangement in the edge region far from the x-points.

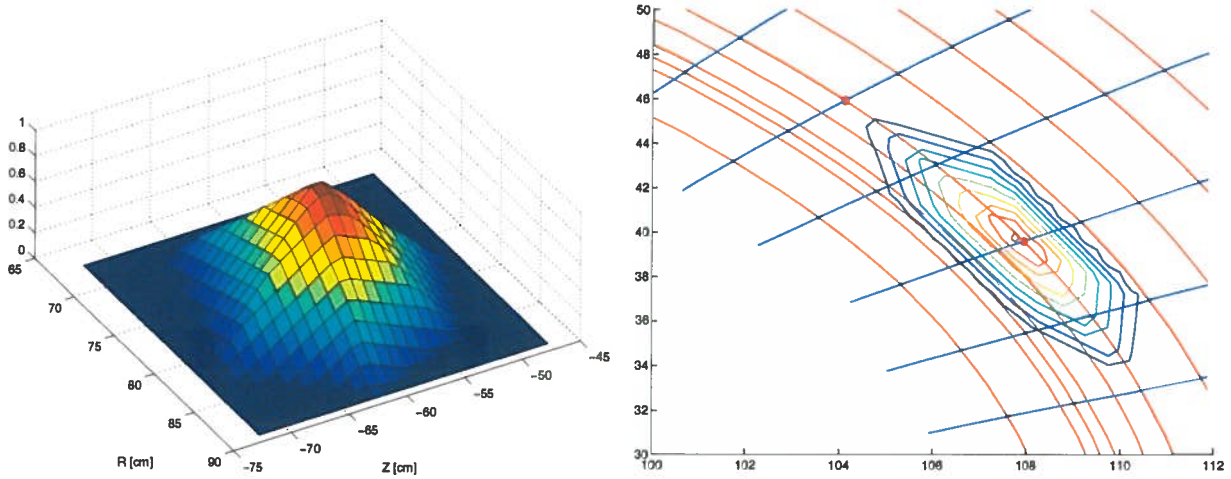

Fig. 6. Examples of base functions in the separatrix base function set. Left: surface view of a hexagonal base function; Right: contour plot of another hexagonal base function along with flux contours.

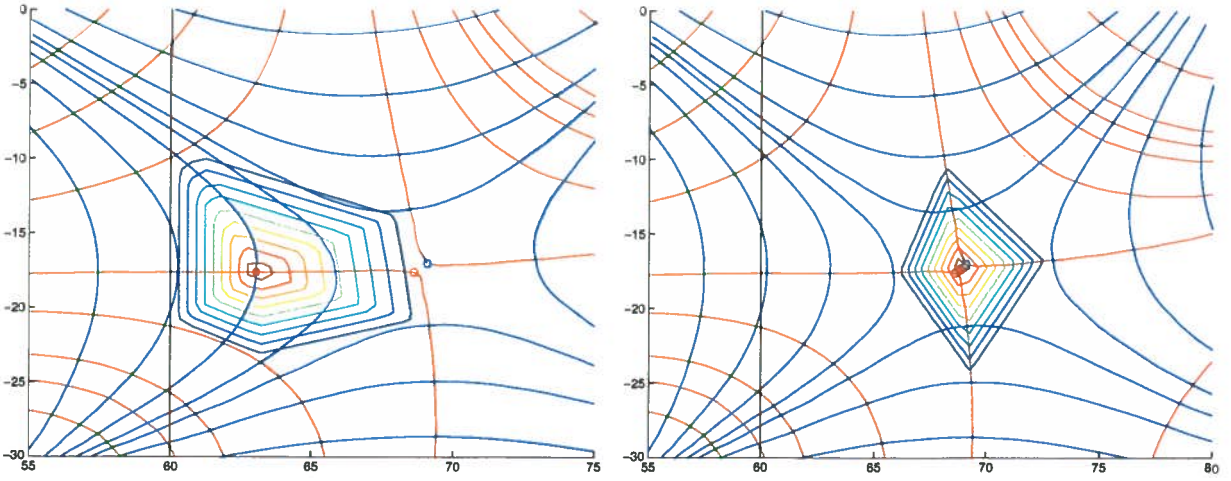

Fig. 7. Examples of base functions in the separatrix base function set. Left: contour plot of a base function next to the x-point; Right: contour plot of the base function at the x-point. Red lines are flux contours, blue ones are gradient lines of the flux.

The base functions of the separatrix function set are generated the following way. The separatrix divides the cross-section of the TCV chamber into 3 regions as shown on *Fig. 8.* Region 3 is the confinement region of the plasma where the field lines are closed. The other two regions are both in the SOL but region 1 lies next to the confinement region while region 2 not. The same regions exist if the magnetic configuration has two x-points but in this case both regions 2 and 1 are cut into two pieces.

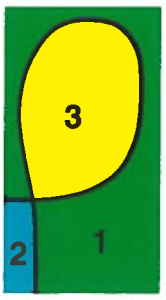

Fig. 8. Flux regions.

In each region flux contours are selected starting from the separatrix at equidistant flux values up to a limiting flux as it is shown on *Fig. 9.* This means a certain number of curves more-or-less parallel with the separatrix on both sides. At predefined distances (`cross point spacing`) along the separatrix gradient lines of the flux are calculated. The crossing points of the gradient lines and the flux contours give a set of points. Starting from the separatrix on every flux contour line alternately the odd or the even points are kept and these form the base point set of the separatrix base function set. The points are connected by straight lines to form triangles and and the triangles around a base point form the edge polygon of the base function belonging to the base point. The triangulation is done in a systematic way in order to form hexagonal base functions similar to the right plot on *Fig. 5* far from the x-point.

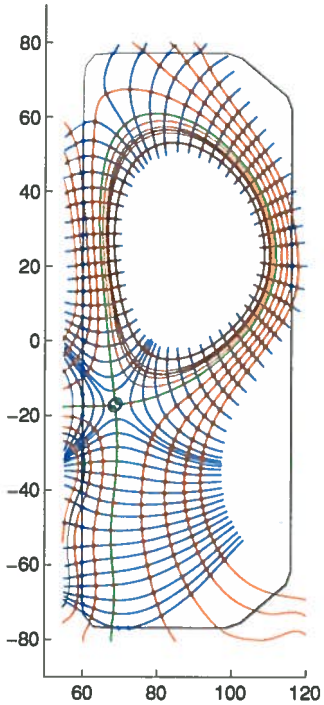

Fig. 9. Grid of the separatrix base function set. The red curves are the flux contours, the blue ones are the gradient lines. The separatrix is plotted in green.

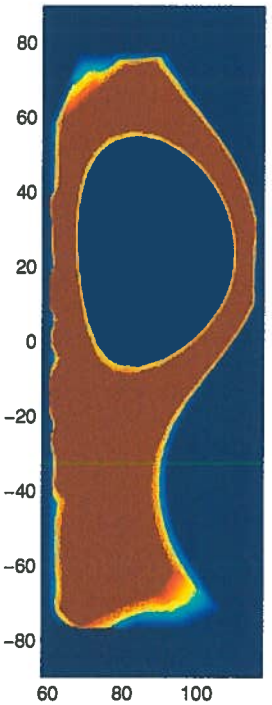

Fig. 10. Sum of all separatrix base functions.

A special problem arises at the TCV vessel wall, where the base functions of the separatrix base function set extend over the wall. As we don't want to allow any radiation intensity outside the chamber the polygons of the base functions are truncated at the wall.

To make sure that the base function set is correctly generated a sum of all base functions is calculated and the result is plotted on *Fig. 10.* As one can see the whole area covered by the base function set has a uniform value. At the wall the system cannot produce a smooth contour as the magnetic configuration does not fit to the wall. Depending on the magnetic configuration this base function set will leave certain areas in the cross-section out, which are so far from the plasma along the magnetic field lines that no radiation is expected there.

The separatrix base function set can represent the radiation around the separatrix. In some cases it is expected that the chamber wall can also act as radiation source. To be able to represent this a third base function set is created. The base points of these base functions are located equidistantly on the wall and their edge polygon is a quadrangle. Two of their points are on the wall (the previous and the next base point) and two are at a predefined width from the wall towards the chamber center. Examples are plotted on *Fig. 11.*

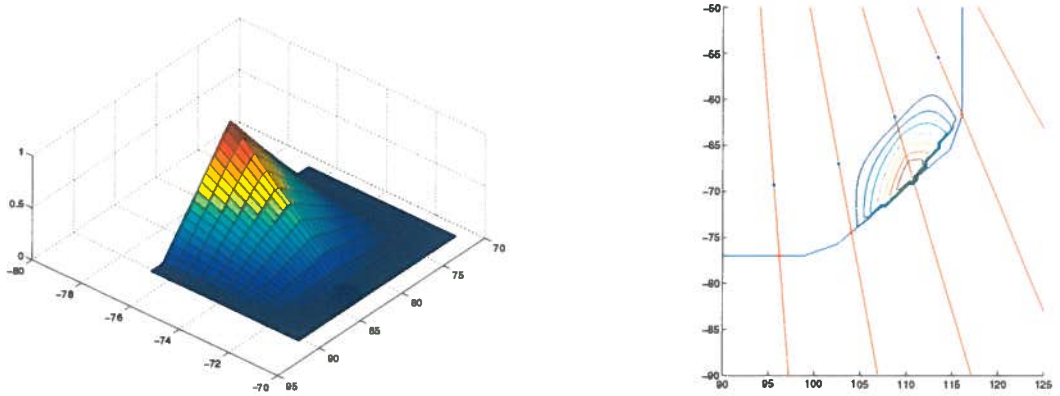

Fig. 11. Two base functions of the wall base function set.

3 Calculation of the measurement matrix

To solve the tomographic problem one needs to calculate the measurement matrix. The elements of this matrix give the signal measured in one bolometer channel in response to a radiation intensity distribution corresponding to one base function. To calculate this matrix first one needs to know the "geometrical function" which describes the detection efficiency of the detection channels in the plasma cross-section.

In previous tomography programs the detectors were considered to measure a simple line integral along their line of sight. In a physical detection system the measurements are not exact line integrals, the finite beam-width effect has to be taken into account. The measurement signal $\hat{f}_i$ of the i-th detector can be calculated as

$$\hat{f}_i = \int_V \int_{F_i(x,y,z)} \frac{\sin\theta}{4\pi r^2} g(x,y,z) dF dV \tag{1}$$

where x, y, z are space coordinates, dF is a surface element on the detector, r is the distance from dF to (x, y, z), $F_i(x, y, z)$ is the area of the detector seen from the (x, y, z) point, θ is the angle between the detector surface and the line of sight and $g(x, y, z)$ is the emissivity. If the emissivity does not change in the z (toroidal) direction, the viewing angle is narrow in the z direction and θ is approximately constant over F_i, the above expression can be integrated over the detector surface and the integral in the z direction can be done separately:

$$\hat{f}_i = \int_x \int_y \left[\frac{\sin\theta}{4\pi r^2} \int_z A_i(x,y,z)dz \right] g(x,y)dxdy, \tag{2}$$

where $A_i(x,y,z)$ is the area of the i-th detector as seen from (x,y,z). Integrating $A(x,y,z)$ over z we arrive to

$$\hat{f}_i = \int_x \int_y K_i(x,y)g(x,y)dxdy. \tag{3}$$

This way the 3–D problem is reduced to a 2–D one. $K_i(x,y)$ is the geometrical function of the i-th detector. Some examples are shown on *Fig. 12.* The detector signals in the tomography program are calculated using Equation (3). The $K_i(x,y)$ geometrical functions are calculated only once and stored in data files. They need to be recalculated using the Matlab command `calc_all_raumwin` only if the measurement geometry changes.

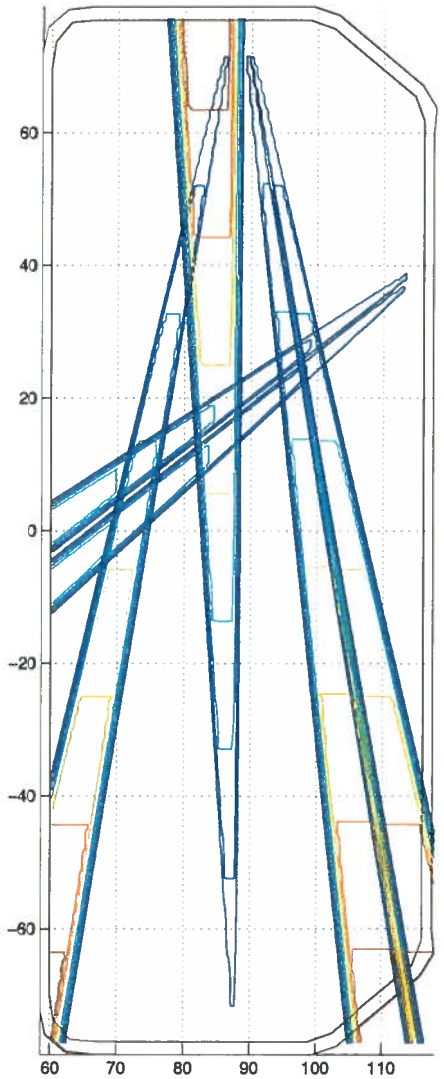

Fig. 12. Contour plot representation of the geometrical function times r^2 of some detectors

To test the geometrical function calculation a comparison with theoretical calculations was done the following way. If in the viewing area of a detector the emissivity does not change significantly perpendicularly to the detector line of sight the integral is reduced to a line integral.

$$\hat{f}_i = E_i \int_l g(x,y)dl \tag{4}$$

where E_i is the Etendue of the detector

$$E_i = \int K(x,y)df. \tag{5}$$

The integral df is over the surface perpendicular to the line of sight of the detector. The Etendue is conserved, it is independent of the distance from the detector. For a pin–hole system

$$E_i = A_a A_d dsin(\theta)/4\pi \tag{6}$$

where A_a is the area of the aperture, A_d is the area of the detector, d is the distance between the aperture and the detector, θ is the angle between the detector surface and the line of sight.

These theoretical Etendue values are compared to the values numerically integrated from the geometrical function. *Fig. 13.* shows some examples. Far from the detector the theoretical value is precisely reproduced. Close to the detector the finite spatial resolution of the calculation results in about 10% fluctuation of the numerically calculated values. However, in front of the apertures no radiation is expected thus these fluctuations cause no problems in the tomography.

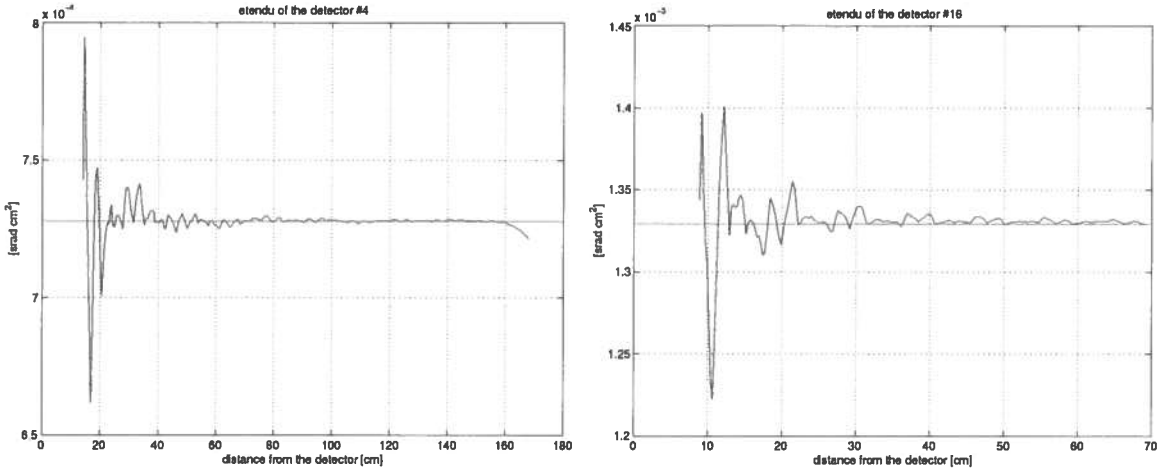

Fig. 13. Variation of the Etendue and its theoretical value (red curve) along the line of sight of two detectors.

Knowing the geometrical function the measurement matrix is calculated as

$$M_{ij} = \int_x \int_y K_i(x,y) b_j(x,y) dxdy. \tag{7}$$

M_{ij} is the signal in the i-th detector in response to a radiation source of the j-th base function.

4 Reconstruction method

The twodimensional radiation distribution is approximated by a weighted sum of the base functions:

$$g(x,y) = \sum_{i=1}^{n} P_j b_j(x,y), \tag{8}$$

P_j we call the parameter vector. The measured signals can be calculated as

$$S_i = \int_x \int_y g(x,y) K_i(x,y) dxdy \tag{9}$$

Substituting Eq. 8 into this expression one arrives at a linear system of equations which connects the parameter vector and the measured signals:

$$S_i = \sum_{j=1}^{n} M_{ij} P_j. \tag{10}$$

The parameter vector P_j can be obtained by solving this equation system. As M_{ij} is not a quadratic matrix the system of equations can have zero, one or many solutions depending on the base function system. In most cases the number of parameters (= the number of base functions) is larger that the number of measurements and the linear equation system always has a solution. (Provided the rank of matrix M_{ij} is greater than the number of measurements.) To select one solution out of the many mathematically possible ones regularisation techniques are used[1].

The regularisation technique used for the TCV bolometer tomography system is described in detail in [2]. The basic idea is that no exact solutions are searched for the linear system of equations but only

$$\frac{1}{m} \sum_{i=1}^{m} \frac{\left(S_i - \sum_{j=1}^{n} M_{ij} P_j\right)^2}{\sigma_i^2} = \chi^2 = 1 \tag{11}$$

is required, where σ_i is the error of the i-th measurement and m is the number of measurements. The σ_i errors should be determined in a realistic way, the quality of the fit largely depends on a correct error estimate. This is very similar to fitting problems, if the error estimate is too small the program will attempt to fit the measurement noise, if it is too high small structures will disappear from the profile. It has to be noted that non-systematic calibration errors can (and should) also be handled as measurement noise. E.g. if the detector sensitivities are calibrated to 5%, it means that statistically the measured signals will have 5% noise which has to be taken into account in the reconstruction.

Additionally to $\chi^2 = 1$ the integral of the square of the derivatives of the radiation profile is minimised:

$$\int_x \int_y \left(\frac{\partial \sum_{j=1}^{n} P_j b_j(x,y)}{\partial x} \right)^2 + \left(\frac{\partial \sum_{j=1}^{n} P_j b_j(x,y)}{\partial y} \right)^2 dxdy = min, \tag{12}$$

where $b_j(x,y)$ is the $j-th$ base function.

Technically these requirements are fulfilled by an iterative solution, details are described in [2]. It also proved to be very useful to limit the radiation intensity to positive values. This can easily be achieved if the base functions are positive everywhere and the P_j parameter values are kept positive.

The correct determination of the error estimates for the channels is very important for the use of the algorithm. The reconstruction starts by first calculating χ^2 for all $P_j = 0$. If this χ^2 is smaller that unity it means that the uniformly zero distribution fits the data within error bars and no reconstruction is attempted. This can happen if the error estimates are far too high or the radiation is too low compared to the measurement noise level. As a second test the minimum of χ^2 as a function of the P_i parameter vector is also calculated. If this is above unity there is surely no solution to the problem. This can happen either if the error estimates are too low compared to the noise (and calibration error) in the measurement or if the actual radiation profile cannot be reproduced by the given base function set.

5 Reconstruction tests

5.1 Radiation profiles composed of base functions

Several numerical tests were performed to test the reconstruction technique. Radiation profiles were generated and the measurement signals were calculated from them numerically. Noise was added to the measurement signals and these "experimental data" were used as input to the calculation. These simulation were done with the Matlab program `tomo_test.m`, the test radiation profiles are in `test_func.m`.

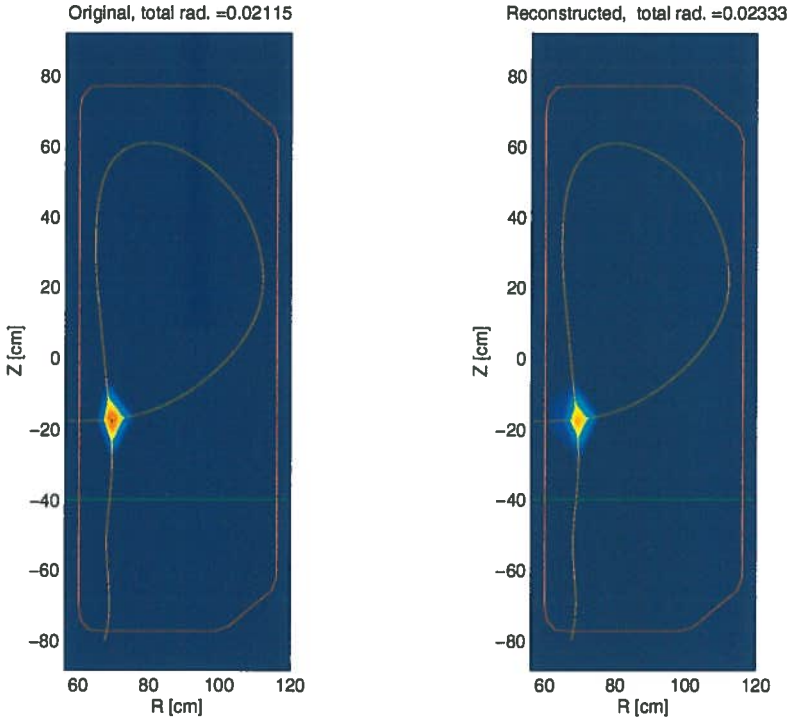

Fig. 14. Reconstruction of a source at the x-point with 1% absolute and 1% relative error.

First, radiation profiles were generated by summing up some base functions. *Fig. 14.* shows an example where the base function at the x-point was used as input radiation profile. The noise added to the measurement (and also the σ_i errors in the reconstruction) were 1% of the highest measurement signal (absolute error) and an additional 1% of the actual measurement signal (relative error). The similarity of the original and the reconstructed profiles is very good, the reconstructed total radiation is higher only by about 10%. This 10% increase is in the low

amplitude fluctuations in the whole cross-section. The peak itself is slightly wider and lower than the original, but its integral is the same to about 1%. It has to be noted, that the σ_i error values has to correspond to the actual measurement noises. As in other fitting problems as well, if the error estimates are too low there is no fit to the data. If they are too high the reconstructed profile is oversmoothed and the radiation intensities are too low.

The 1% relative error is unrealistic as the calibration errors of the measurement channels act also as a source of error and the bolometer channels are not calibrated to 1% precision. Another reconstruction with the same radiation profile but with 10% relative and 1% absolute error is shown on *Fig. 15.* The peak became wider and its integral is 25% lower than the original. This is due to the fact that the regularisation selects solutions which are "smoother", this way it reduces the peaks.

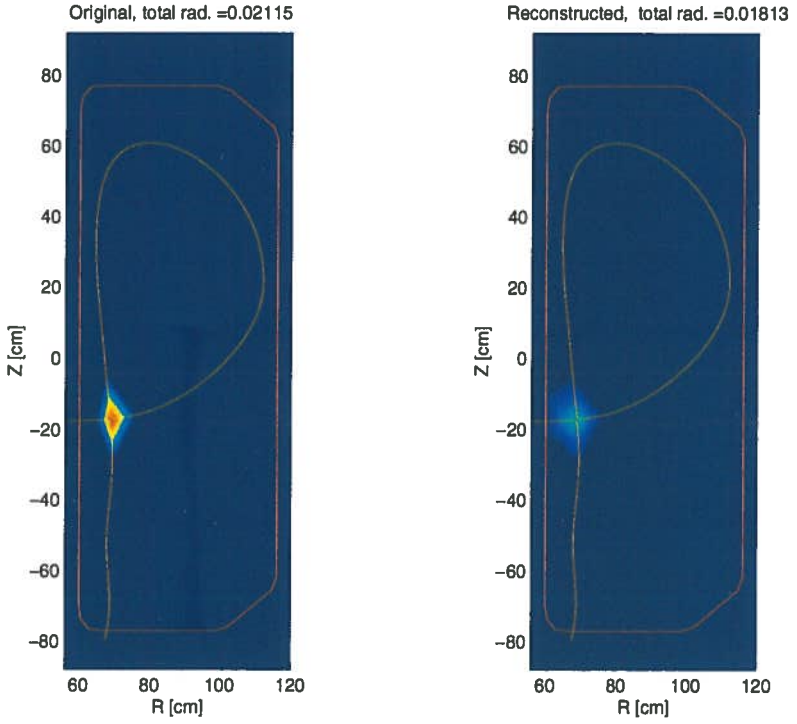

Fig. 15. Reconstruction of a source at the x-point with 1% absolute and 10% relative error.

The reconstruction of a radiating belt at the separatrix is shown on *Fig. 16.* The original radiation profile was constructed by adding all the base functions at the separatrix and the reconstruction was done with 1% absolute and 5% relative error (noise with the corresponding amplitude was added). The structure of the radiation profile is clearly reconstructed, but the width at the narrow parts is not. This is simply a reflection of the fact that the bolometer system does not have the necessary resolution to measure such narrow profiles.

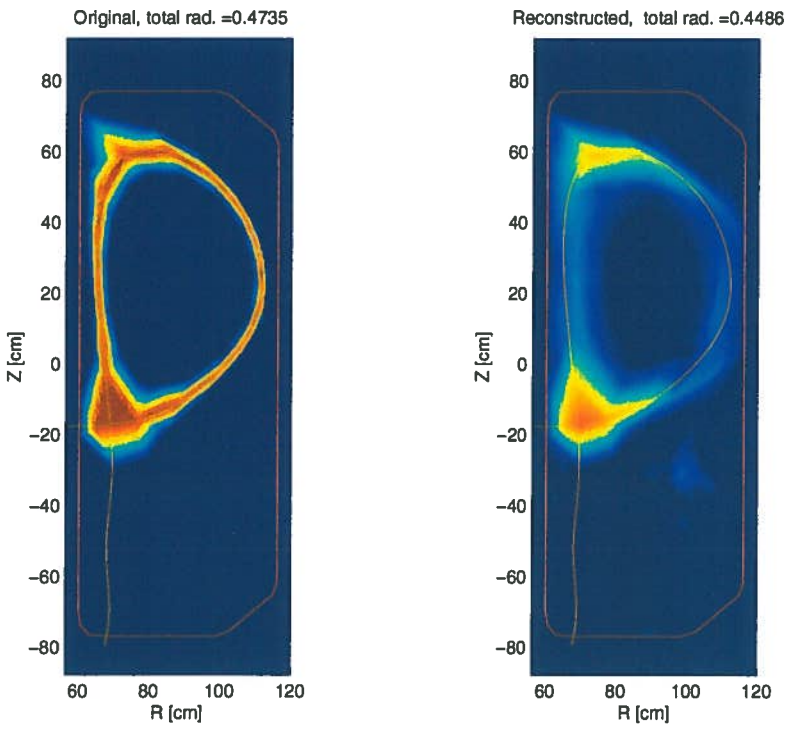

Fig. 16. Reconstruction of a radiating belt with 5% absolute and 1% relative error.

Various other profiles were generated and used for reconstruction tests with similar results. One more example is shown here to indicate that radiation at the x-point and on the wall close to it can be distinguished. *Fig. 17* shows a test result where the radiation intensity was generated by using two base functions at the wall. The reconstruction clearly indicates that radiation comes from the wall and not from the x-point.

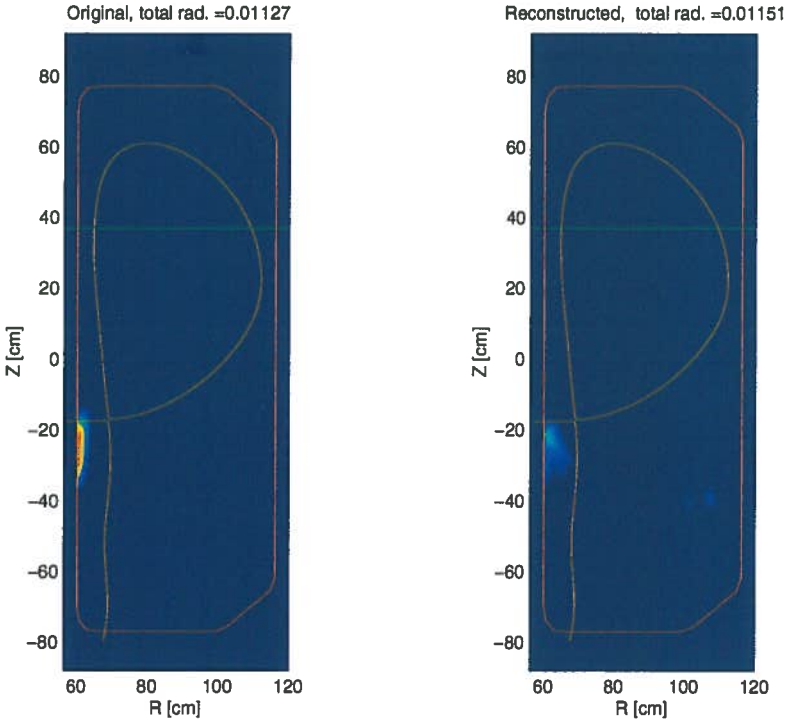

Fig. 17. Reconstruction of local radiation at the wall with 3% absolute and 3% relative error.

It has to be noted that one case was found where the radiation profile could not be adequately reconstructed, namely when the wall was assumed to radiate uniformly everywhere. In this case there are several regions in the cross-section where the radiation is seen by only one or no detector and the reconstruction cannot localise the position of the radiation in these cases.

5.2 Other radiation profiles

If arbitrary radiation profiles are processed with the test program it cannot be assured that a solution is found. This is due to the fact that the base function set limits the possible radiation profiles. With such special base function set the resolution is highly dependent on the location an direction in the cross-section. For example in the plasma center it is assumed that the radiation changes smoothly, thus the resolution of the central base function set is kept low. If a small localised source is placed there the tomography program cannot represent the distribution. This manifests itself by the fact that χ^2 cannot reach 1, it is always above it. On the other hand if the source can be represented within error bar than a result is obtained and it is usually a relatively good approximation of the original source. An example is shown on *Fig. 18.* The original source was a Gaussian peak. The reconstructed one is rather close to it, but of course it is not as smooth as the given base functions cannot represent a source like the original smoothly. If a similar but much narrower peak is used as input the reconstruction fails as the size of the base functions in the direction of the magnetic flux contours is too big to represent it.

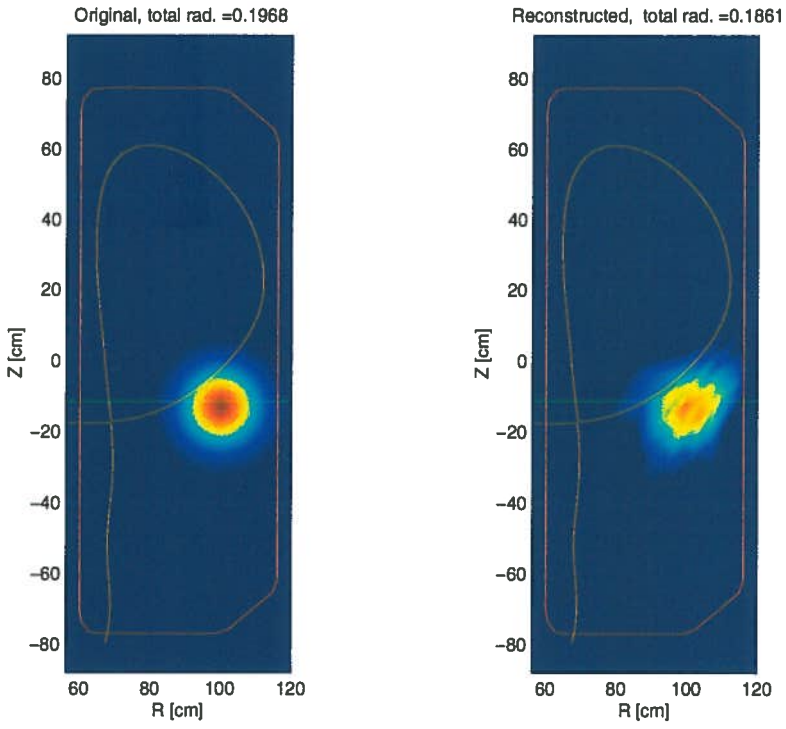

Fig. 18. Reconstruction of a Gaussian radiation peak with 1% absolute and 5% relative error.

6 The effect of neutral particles

It is suspected that part of the bolometer signals might originate from neutral particles. If this is the case the tomographic reconstruction might be severely affected as neutral particles cannot penetrate through the hot regions of the plasma. If a source of neutral particles is present somewhere at the plasma edge, the bolometers looking directly to that edge region will detect the particles, while on the other side of the plasma the detectors won't see it. This effect will certainly distort the reconstructed profile.

To simulate this behaviour two input radiation profiles were taken as input to the numerical simulation. One is a normal radiating source and measurement signals are calculated the normal way. The other was assumed to be a source of neutral particles It was assumed that these neutrals have a certain λ mean free path in the plasma, thus their intensity was multiplied by $e^{-d/\lambda}$ where d is the length of the path the neutrals cover within the separatrix to reach from the source to the detector. For the sake of simplicity λ was fixed to 10 cm. Although this seems to be a rather rough estimate but as λ is considerable smaller than the plasma size it is not very important whether it is 5 or 20 cm. The detectors on the other side of the plasma will not see the particles, the difference would manifest itself only for a few detectors at some special angle from the source.

First a pure neutral particle source was placed at the x-point. Reconstruction was attempted with 1% absolute and 5% relative error but no fit was found to the data. Part of the source was replaced by a true radiation source of the same shape and location. A result could be obtained only if 75% of the source was radiation. The tomographic reconstruction in this case was practically the same as the one on *Fig. 14.* with about 20% less total radiation than in the original profile (including the neutrals) that is the radiation profile was more-or less correctly reconstructed. Of course this behaviour depends strongly on the value of error given in the reconstruction. If higher error bars are allowed than the reconstruction tolerates such problems as the neutral source more. If the channels were very precisely calibrated and noises were small the tomography program could easily sort out any discrepancies in the measurement like the neutral particles.

Various other combined neutral-radiation profiles were tested and in all but one case similar result were obtained: no reconstruction could be achieved if the neutral source was higher than 25% of the total radiation. The only exception is the case of a uniformly emitting separatrix, as shown on *Fig. 19.* For this source a result was obtained even for 75% neutral source, but the reconstructed total intensity is only about half of the original one, that is twice the radiation without neutrals. This result can easily be understood. The bolometer channels all see only radiation from that part of the ring which is closer to them. This is about half of the signal they would measure for a true radiating source.

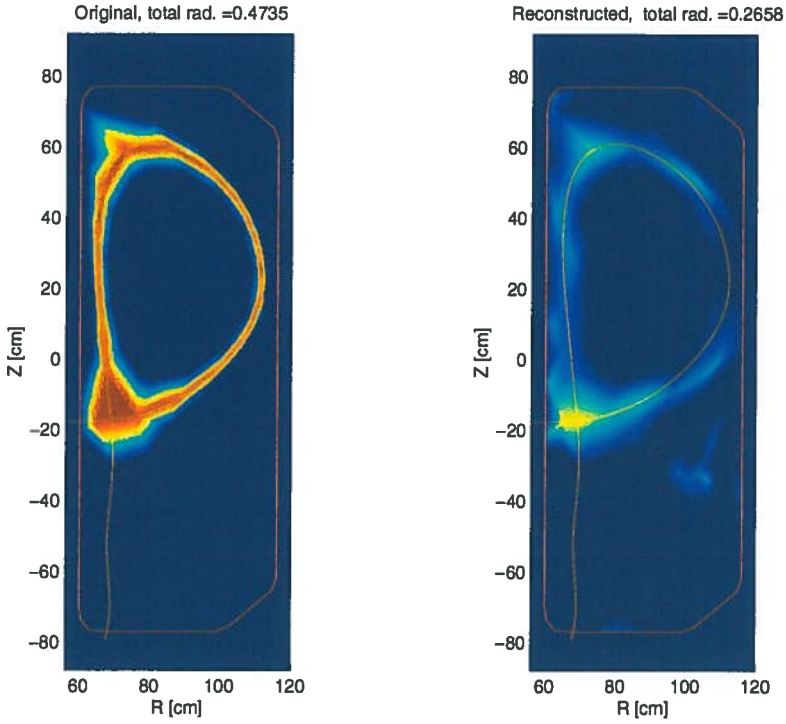

Fig. 19. Reconstruction of a radiating ring with 75% of the radiation in neutrals.

In the next step differently shaped neutral and true radiation sources were applied. *Fig. 20.* shows an example where a strong (3 × radiation) amplitude neutral source was placed on the wall. The reconstructed image shows the source but with smaller amplitude and the radiation part is not effected very strongly.

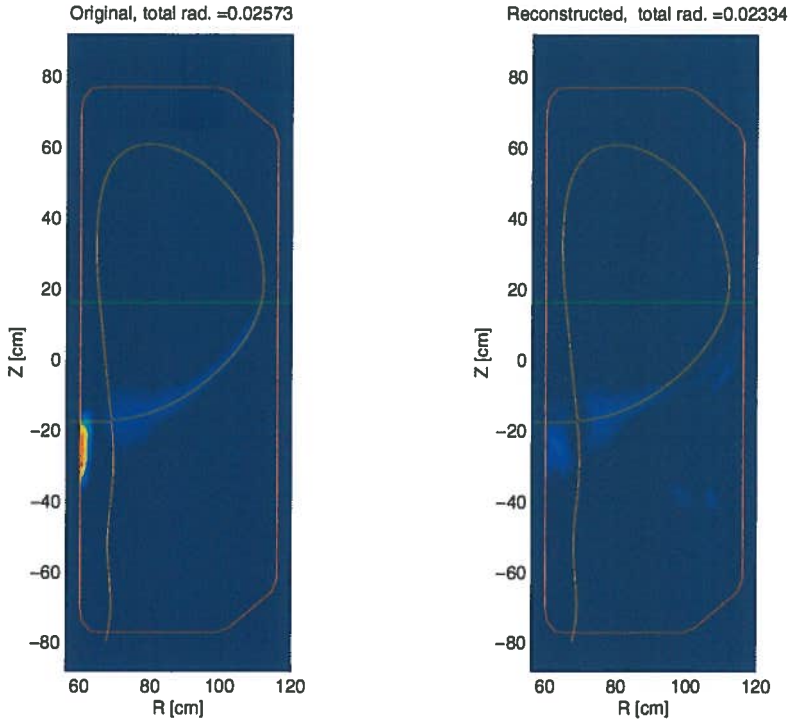

Fig. 20. Reconstruction of a radiation source with and additional neutral source on the wall.

To summarise the results of the simulation of the effects of neutral particles it can be said that purely neutral particle sources are marked as bad measurements by the tomography

program. If the fraction of neutral particles is only around 25% of the total radiation the profiles are reconstructed and the reconstruction corresponds nearly to the true radiation source. The only exception is when the whole separatrix acts as a source of neutrals, because in this case the the radiative part of the profile is strongly overestimated. If an additional neutral peak is added to the true radiation profile it does not effect the reconstruction of the radiation strongly, but appears as a radiation source itself albeit with reduced amplitude.

7 Reconstruction of plasma discharges

Radiation profiles for several plasma discharges were calculated. The results are stored on the MDS+ database. As an example the results from different time instances of a single discharge are presented here on *Figs. 21-22.* These were obtained by taking into account the change in magnetic geometry in time. The base function set was calculated for every fifth time instance. Three intensity distributions are shown on *Fig. 21.*

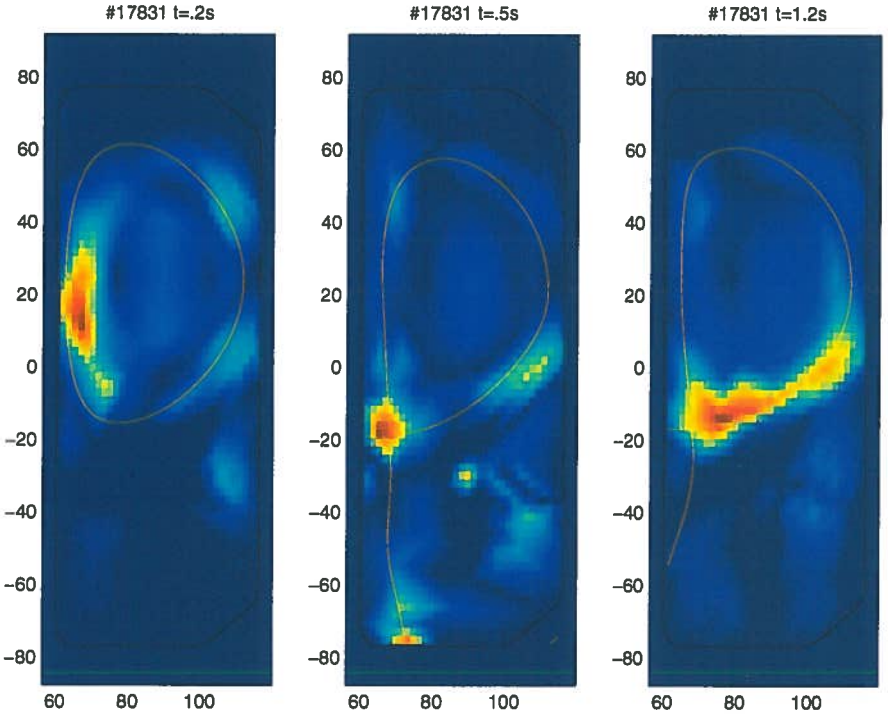

Fig. 21. Radiation intensity profiles reconstructed from experimentally measured bolometer signals.

The total radiated power and the power radiated inside and outside of the LCFS can easily be calculated from the reconstruction results. As the reconstruction is fast if the magnetic geometry is fixed one can obtain these parameters with good temporal resolution. An example for the time evolution of the total radiated power and the radiation fraction inside the LCFS is shown on *Fig.22.*

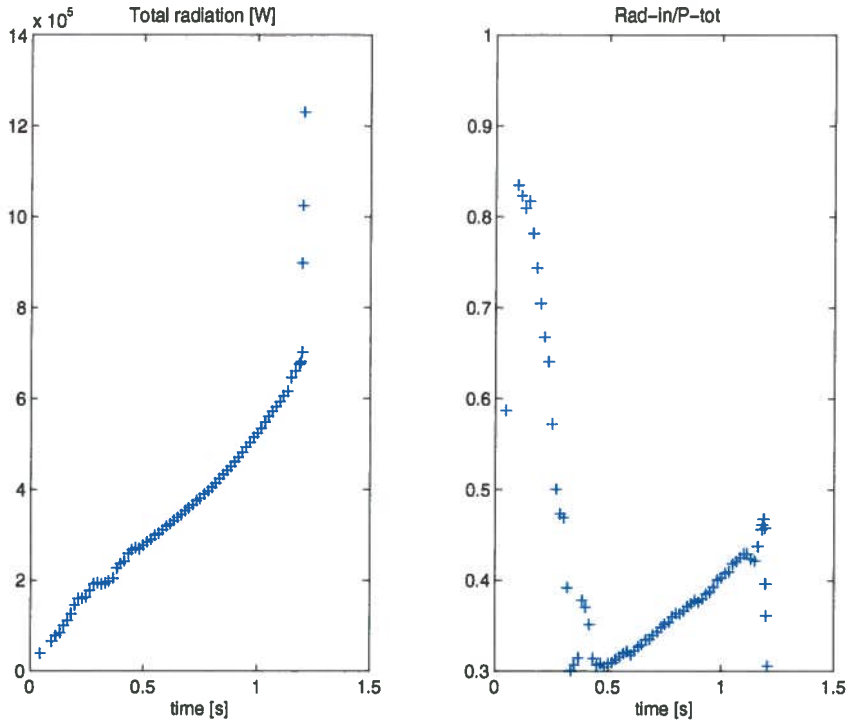

Fig. 22. Time evolution of the total radiation intensity and the fraction of power radiated inside the LCFS as determined from the reconstructed radiation profiles.

8 Using the Graphical User Interface

The graphical user interface (GUI, see *Fig. 23*) of the flux-base bolometer tomography program starts from the general bolometer tomography graphical user interface. Most of this window serves for controlling the settings and calculation of the base function set, only the lower sub-window serves for the inversion (reconstruction) of the radiation profiles.

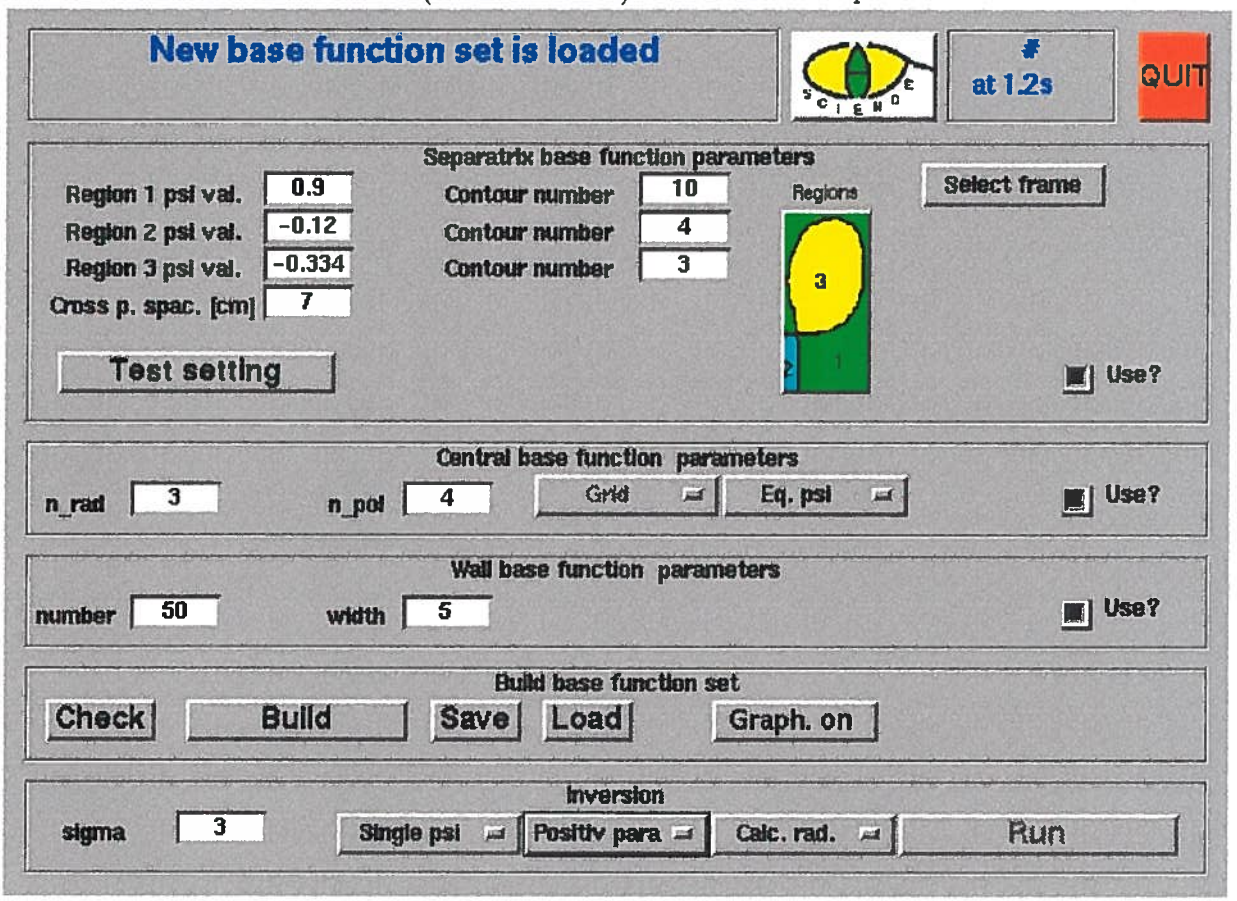

Fig. 23. The graphical user interface of the flux-base bolometer tomography.

A time instance can be selected from the ones set in the general bolometer tomography GUI by using the "`Select frame`" button. The magnetic geometry in this time instance will be used for the construction of the base function set for all time instances if the "`single psi`" method is selected in the inversion sub-frame (see below).

The base function system settings can be adjusted in the upper three windows, which are connected to the three base function sets within the whole base functions system as described in section 2. Each of the base function sets can be individually enabled/disabled by checking the checkboxes on the right. For the separatrix base function set first the limiting flux values of the three regions should be set ("`Region x psi val`"). The numbering of the regions is shown on the small colour illustration in the window. As the flux has a value of 0 on the separatrix the closer the limiting flux values are to zero the closer the base functions will be located to the separatrix. In region 2 the limiting flux should be positive, while in the other two regions it is negative. The "`Contour number`" setting right to each limiting flux indicates how many flux contours will be used in the given region. This value includes the contour *on* the separatrix as well, thus it has to be greater than 1. The "`Cross p. spac.`" (cross point spacing) setting changes the spacing (in cm) of base functions along the flux contours on the separatrix. The

resolution far from the separatrix can be either smaller or higher depending on the curvature of the separatrix. This parameter defines the resolution of the tomography algorithm along the flux contours. It should be the same for all regions to ensure correct fit of the functions at the separatrix, thus it can be set for all three regions at the same time. The settings can be verified graphically by pressing the "`test setting`" button.

The next window controls the parameters of the central base function set. This base function set is identical to the base function set of the x-ray tomography, but only the "grid" type is implemented to allow limiting the radiation intensity to positive values, thus the "`Grid`" control is made inactive. The method of arrangement of the flux contours can be selected by the "`Eq. psi`" control, "`n_rad`" sets the number of radial zones, "`n_pol`" the number of base functions in one zone. As the total radiation is expected to be low and nearly constant along flux contours in the plasma center, the poloidal resolution can usually be kept low.

The wall base function parameters are set in the third window. It is only the number of the functions (they will be arranged equidistantly along the wall) and the width in cm.

A consistency check can be performed for the parameters with the "`check`" button and the calculation can be started by pressing the "`build`" button. If the "`Graph`" button shows on, the generation of base functions can be followed in a graphical window. A complete base function set can be loaded or saved under different names.

Inversion can be controlled in the lowermost sub-window. "`sigma`" sets the percentage noise defined for each measurement channel, that is

$$\sigma_i = \frac{\texttt{sigma}}{100} \times f_i, \tag{13}$$

where f_i is the signal in channel i and `sigma` is the value entered into this window. The droplist button "`single psi`" can be used to decide if a single magnetic geometry is to be used for the reconstruction of all time instances or a base function system is to be built for each. The former solution is much faster but it is applicable only if the magnetic configuration does not change considerably in the timewindow. The next control selects if the radiation intensity should be kept positive. Keeping the solutions positive avoids many solutions which were mathematically possible without any reasonable physical meaning. If "`calc. rad.`" is switched on, the total radiation intensity and radiation fractions in various regions of the plasma will be calculated. The "`Run`" button starts the inversion. The results can be stored in the general bolometer tomography GUI.

9 Program routines

The table below is a short overview of main Matlab program routines of flux–based bolometer tomography. These routines are commented and can be used to perform special tasks (e.g. automated data processing) which cannot be performed with the GUI.

function	*description*
`grid_flux_gui.m`	The graphical user interface.
`grid_flux_tomo.m`	Callback routine of the GUI.
`determine_magnetic_conf.m`	Determines the magnetic configuration, number of x-points, LCFS, etc.
`make_mesh_points_f.m`	Creates the mesh points for the base function set.
`combine_mesh_point_f.m`	Arranges the mesh points.
`make_function_sep.m`	Calculates separatrix base function set of the base function system.
`make_base_function_wall.m`	Calculates wall base function set of the base function system.
`make_base_function_cent.m`	Calculates center base function set of the base function system.
`calc_tmat.m`	Calculates the measurement matrix.
`calc_hmat.m`	Calculates the H regularisation matrix.
`regulo_2d_flux.m`	This is the regularisation (calculation of the radiation profile).
`calc_all_raumwin.m`	Calculates the geometrical functions and stores them in files.
`tomo_test.m`	A well commented example of reconstruction tests.

Several other subprograms and files are needed for successful operation of the flux-based tomography program which are installed on the TCV computers.

References

[1] M. Anton, *et al.* X-ray tomography on the TCV tokamak *Plasma Phys. Control. Fusion* **38** 1849 (1996)

[2] S. Zoletnik, S. Kálvin A method for tomography using arbitrary expansions *Rev. Sci. Instrum.* **64** 1208 (1993)